Korean J. Chem. Eng., **28**(8), 1672-1676 (2011)
DOI: 10.1007/s11814-011-0034-4

Electrocatalytic properties of Fe-based bulk metallic glasses for hydrogen evolution reaction

Shan Lin Wang*, Dong-Hyun Kim, and Seonghoon Yi*,†**

*Department of Materials Science and Metallurgy, Kyungpook National University, Daegu 702-010, Korea
**Department of Chemical Engineering, Kyungpook National University, Daegu 702-010, Korea
(*Received 17 January 2011 • accepted 15 February 2011*)

Abstract−The electrocatalytic activity of newly developed Fe-based bulk metallic glasses was evaluated by polarization and impedance measurements in deaerated 1 M KOH solution at room temperature. The electrocatalytic activity as well as the glass-forming ability of the $Fe_{73}C_3Si_{7.3}B_{8.5}P_{5.7}Mo_{2.5}$ alloy was improved by the partial substitution of Fe with 13.5 at% Co. In hydrogen evolution reaction, the metallic glasses exhibited higher activity than the activity of G14 ($Fe_{60}B_{10}Si_{10}Co_{20}$) metallic glass, which has been reported to be comparable to the activity of Pt electrode. The activity was further improved after a chemical pretreatment in 1 M HF solution for 1 min due to the formation of cobalt-rich layer with a large effective surface area.

Key words: Fe-BMG, Electrocatalytic Activity, Hydrogen Evolution Reaction, Pretreatment

INTRODUCTION

As a clean fuel potentially replacing crude oil, hydrogen is of interest. To produce hydrogen cost-effectively by electrolysis, the development of an electrode having a low overpotential in hydrogen evolution reaction (HER) is one of the key issues. In this regard, Fe-based metallic glasses merit attention.

Fe-based metallic glasses have a large flexibility in their chemical composition when compared to crystalline alloys and exhibit high reactivity for their metastable states and unique atomic structures having a short-range order. Since the first report of Fe-based metallic glass as a catalytic material in 1981 [1], a number of investigations have been focused on the synthesis of Fe-based metallic glasses for catalytic applications, such as ammonia synthesis [2], acetylene hydrogenation [3], CO hydrogenation [4-6] and hydrogenation [7]. On the other hand, the metallic glasses also showed good electrocatalytic activities, and the activities were further improved by the pretreatment in an acid solution such as HF, HCl or HNO_3 [8-10]. The improved electrocatalytic properties were attributed to changes in the surface compositions and/or surface area by the pretreatment. An Fe-based metallic glass, known as G14, with an atomic composition of $Fe_{60}B_{10}Si_{10}Co_{20}$ has been reported to have electrocatalytic activity comparable to Pt electrode [7,11] in HER. The Tafel slopes of G14 and Pt electrodes are −95 mV/dec and −120 mV/dec in room temperature, respectively. However, extensive applications as catalytic materials of the previous Fe-based metallic glasses have been limited partially due to the lack of glass-forming ability and high production cost.

In this study, novel Fe-based bulk metallic glasses (BMG) with atomic compositions of $Fe_{73}C_3Si_{7.3}B_{8.5}P_{5.7}Mo_{2.5}$ (BMG1) and $Fe_{59.5}C_3Si_{7.3}B_{8.5}P_{5.7}Mo_{2.5}Co_{13.5}$ (BMG2) have been developed and studied for hydrogen production applications. The BMGs have excellent glass-forming ability and can be produced cost effectively in large quantities. The electrocatalytic activity of the BMGs in HER was evaluated by polarization and impedance measurements in 1 M KOH solution at 25 °C. The electrocatalytic properties of the BMGs were compared with those of G14.

EXPERIMENTAL

The master ingots were prepared by arc melting in an argon atmosphere using cast iron, industrial ferroalloys and commercial grade elements. The chemical compositions including the oxygen contents of raw materials are shown in Table 1. To achieve chemical homogeneity, the ingots were remelted at least four times and then were suction-cast into a copper mold under argon atmosphere to fabricate the cylindrical rods with the dimension of ϕ (2-8)×L50 mm. In contrast, G14 has not enough glass-forming ability to be fabricated as a glassy rod, and only glassy ribbons with the thickness of ~40 μm and the width of ~10 mm can be prepared using a single roll melt spinning equipment. The crystallinity of the samples was identified using x-ray diffraction (XRD, Philip X'Pert diffractometer) with Cu radiation (Cu-Kα, λ=0.1541 nm). The differential scanning calorimeter (DSC, Pyris Diamond DSC) was used to investigate the thermal properties and crystallization behaviors of glassy alloys. The electrocatalytic activity of the glassy alloys for HER was studied by a quasi-steady-state polarization technique using a potentiostat with EG&G powersuit software (EG&G Princeton Applied Research PARSTAT 2273, Oak, TN). The potential was swept with a scanning rate of 2 mV/s over the range of −1.5~−0.8 V/SCE (Saturated calomel electrode) to assess the Tafel behavior in 1 M KOH solution at 25 °C under deaerated condition by purging pure N_2 prior to and during experiment. The cyclic voltammetry was carried out at a sweep rate of 50 mV/s between −1.4 to 0.5 V. The electrochemical impedance was measured from 50 mHz to 50

†To whom correspondence should be addressed.
E-mail: yish@knu.ac.kr

Table 1. Chemical compositions (wt%) of industrial raw materials

Materials	C	Si	B	P	Cr	Mn	Ti	Al	Ni	Ca	O	N	S
Fe-C	4.28	0.46		0.20		0.20	0.03		0.09				0.04
Fe-P	0.02	0.01		26.28		0.69	0.35			0.01			0.01
Fe-B	0.17	0.65	19.75	0.04		0.21		0.05			0.02	0.01	
Fe-Cr	1.43	0.33		0.02	55.49						0.24	0.01	

*Commercial pure elements (Al, Si, Mo, Co)>95%

kHz with an alternating voltage of 10 mV.

RESULTS AND DISCUSSIONS

As shown in Fig. 1(a), a halo pattern typical for amorphous phase was obtained from the XRD result of the rod (3Φ) indicating that BMG2 can be prepared as a fully amorphous rod with the diameter of up to 3 mm through a suction casting method. Since the critical cooling rate for amorphization upon solidification decreases with the increase of maximum diameter of fully amorphous rod, it can be inferred that the glass-forming ability tends to be increased by the partial replacement of Co for Fe in BMG1. The amorphous rods of BMG1 and BMG2 crystallize at around 830 K when the heating rate is 40 K/min (Fig. 1(b)).

After pretreatment of the amorphous rods using the 1 M HF solution for 1 min at 25 °C, the phases FeO, $Fe_4(PO_4)_3(OH)_3$ and a small amount of unknown phase(s) were formed on the surface of BMG1, while the phases FeO, (Co, Fe), CoO and some unknown phases were formed on the surface of BMG2 (Fig. 2).

For the characterization of the electrochemical behavior for the as-cast amorphous BMG1 and BMG2 electrodes, the cyclic voltammograms were run between the potential range of the hydrogen and oxygen evolution reactions in 1 M KOH at a sweep rate of 50

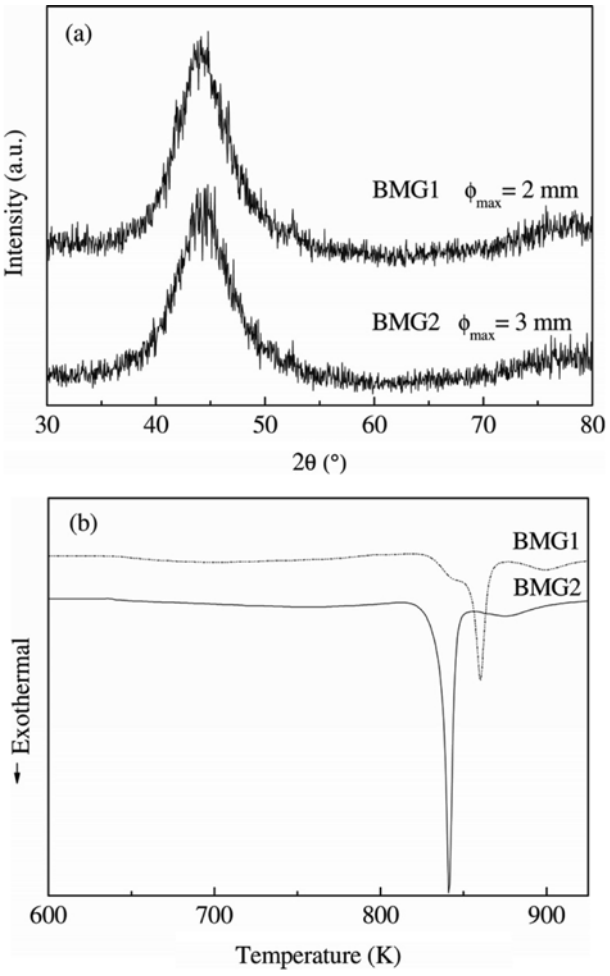

Fig. 1. The thermal results for BMG1 and BMG2: (a) XRD, (b) DSC.

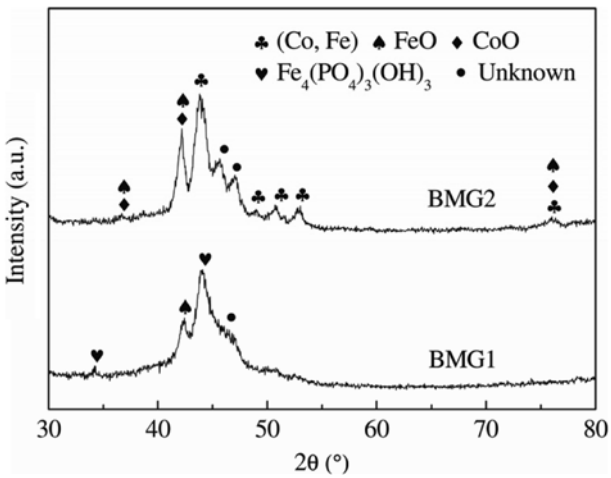

Fig. 2. The results of XRD for BMG1 and BMG2 after pretreatment using 1 M HF solution for 1 min.

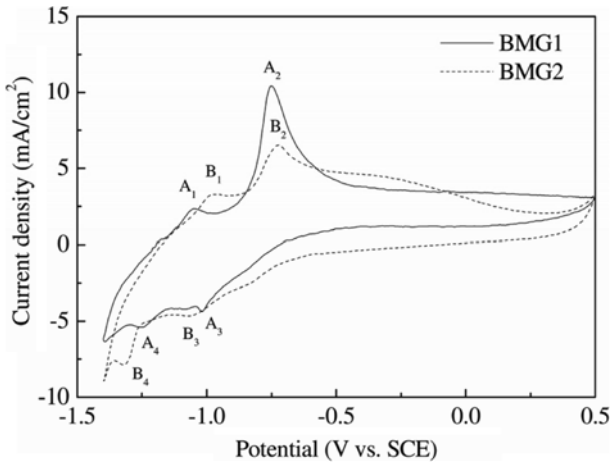

Fig. 3. The results of Cyclic voltammograms for BMG1 and BMG2.

mV/s (Fig. 3). The voltammogram for BMG1 electrode exhibits two anodic oxidation peaks (A_1 and A_2) and two corresponding cathodic reduction peaks (A_3 and A_4). The potentials for the peaks A_1 and A_2 associate with the formations of ferrous hydroxide ($Fe/Fe(OH)_2$) and magnetite (Fe^{2+}/Fe_3O_4), respectively [12,13]. Since the peak potential for the formation of $Co(OH)_2$ is known to be very close to that for $Fe(OH)_2$, simultaneous formation of $Co(OH)_2$ and $Fe(OH)_2$ can be considered during the oxidation event around B1 [12,14]. Moreover, the potential of peak B_1 for BMG2 electrodes increases with a cobalt addition. At the potential of B2, the transition of magnetite is proposed, and the corresponding cathodic reduction for BMG2 occurs at potential of B3 and B4.

Two different types of amorphous electrodes, i.e., as-cast electrode and pretreated electrode, in the 1 M HF solution were investigated for HER. The quasi-potentiostatic curves for the electrodes in the 1 M KOH solution were recorded in the range of −0.8~−1.5 V vs. SCE with a scanning rate of 2 mV/s. The performance of the amorphous electrodes with respect to HER is primarily characterized by the hydrogen overpotential. A linear relationship between the hydrogen overpotential η and the cathode current density i exists [15]:

$$\eta = a + b\log(i)$$

where a is constant, b is the Tafel slope, and the exchange current density $i_0 = 10^{-a/b}$. The Tafel slope is mainly affected by the reaction mechanism. In the case of identical Tafel slope, the exchange current density is mainly affected by the effective surface area.

The typical Tafel plots for two types (i.e., as-cast and pretreated in 1 M HF) of amorphous electrodes BMG1 and BMG2 are shown in Fig. 4 and Fig. 5, respectively. The kinetic data extrapolated from the plots are listed in Table 2. The results of Tafel slope and overpotential when i=250 mV/cm^2 for as-cast BMG1 and BMG2 electrodes exhibit high electrocatalytic activity comparable to G14 alloy that has been known as a good electrocatalytic material for HER, comparable to Pt electrode. The electrocatalytic activity for BMG2 is significantly improved by the pretreatment in the 1 M HF solution, exceeding the electrocatalytic activity of BMG1 as well as G14. It is well known that the electronic density of state for d-electronic transition metals can be increased by a partial substitution of iron with cobalt since the negative heat of mixing of Fe-Co [16], which results in an increase of the availability of metal valence electrons for chemisorptive bond formation, that is, weakening metal-electron donor (M-H) bonds, while strengthening metal-electron acceptor (M-OH) bonds [17,18], which means an improvement of electrocatalytic activity for HER. A notable improvement of electrocatalytic activity of BMG2 after pretreatment can be attributed to the formation of a cobalt-rich layer with a large effective surface area [8], since boron and phosphorous are selectively leached from the alloy surface [4,19].

The electrochemical impedance spectroscopy (EIS) is applied to further investigate the electrode/electrolyte interface and the corresponding process that occurs at the electrode surface. The impedance data for HER at η of −50 mV in 1 M KOH solution at 25 °C are shown in Fig. 6. The data can be fitted to the corresponding lines using nonlinear-least-square fit analysis software. Also, the equiva-

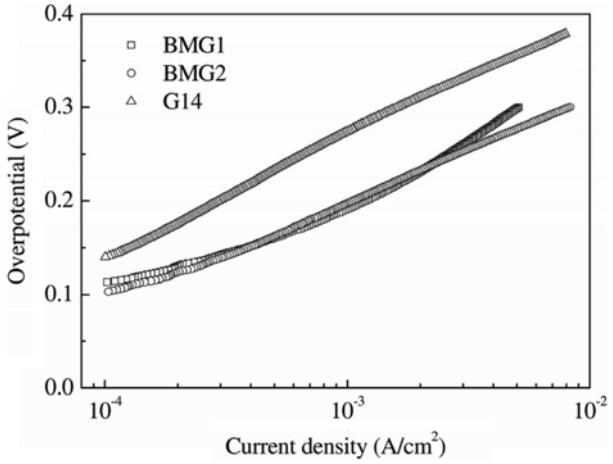

Fig. 4. Tafel plots of BMG1, BMG2 and G14 at as-cast state.

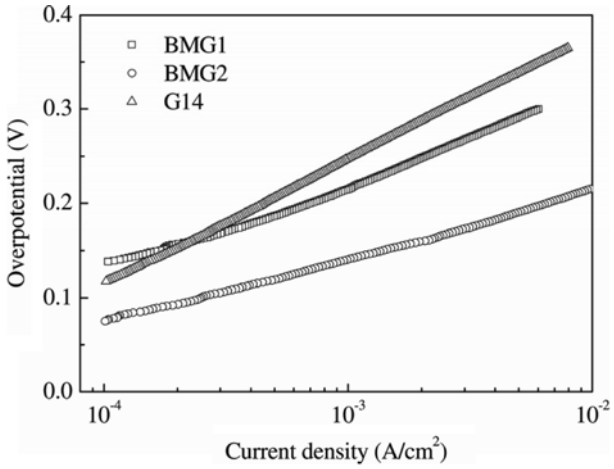

Fig. 5. Tafel plots of BMG1, BMG2 and G14 after pretreatment using 1 M HF solution for 1 min.

Table 2. Kinetic results of the glassy alloys for HER in 1 M KOH

Alloy	Condition	η_{250} (mV)	−b (mV/dec)	i_0 (mA/cm^2)	R_{ct} (Ωcm^2)	C_{dl} (F/cm^2)
BMG1	As-cast	476	115	1.4×10^{-2}	632	3.2×10^{-5}
	1 M HF	455	98	5.7×10^{-3}		
BMG2	As-cast	462	110	1.6×10^{-2}	204	9.0×10^{-5}
	1 M HF	306	69	9.2×10^{-3}		
G14	As-cast	559	121	6.0×10^{-3}		
	1 M HF	553	128	1.1×10^{-2}		

* η_{250} is the overpotential when the current density is 250 mA/cm^2

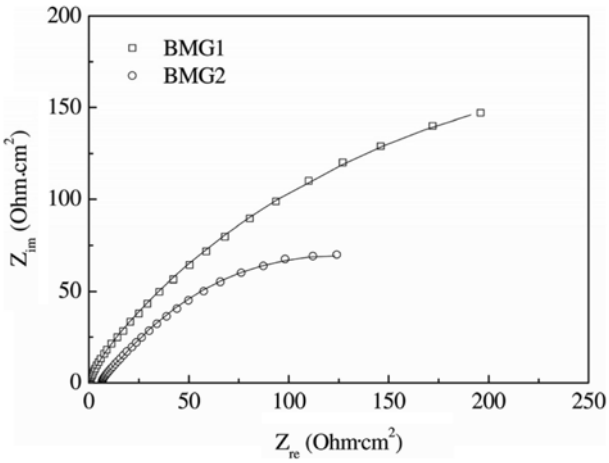

Fig. 6. Nyquist plots for BMG1 and BMG2 at η=−50 mV vs. SCE.

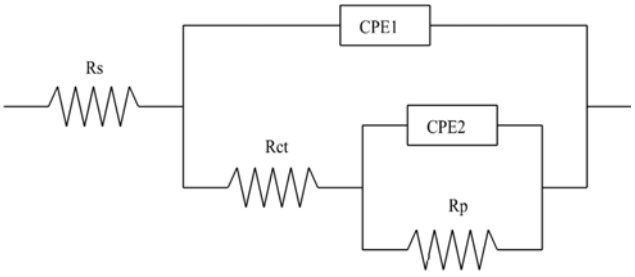

Fig. 7. Equivalent circuit for the fitting of impedance results.

lent circuit and the parameters obtained from the nonlinear-least-square fit analysis results are shown in Fig. 7 and Table 2, respectively. As can be expected from the polarization experiment results, the double layer capacitance C_{dl} of BMG2 is larger than that of BMG1, while the charge transfer resistance R_{ct} is smaller than that of BMG1. The increasing tendency in C_{dl} and R_{ct} for BMG1 and BMG2 agrees with that of current density, indicating the enhanced HER kinetics of BMG2 [20,21].

A fairly good linear relationship between $\log R_{ct}^{-1}$ vs. overpotential can be obtained as shown in Fig. 8. The exchange current densities were derived from the intercepts of these lines at zero overpotential according to the equation [21,22]

$$i_0 = \frac{RT}{zFR_{ct}}$$

where R is the gas constant, F is the Faraday constant, T is the absolute temperature and z is the number of electron transferred. The exchange current densities of 3.0×10^{-2} and 7.4×10^{-2} mA/cm^2 for BMG1 and BMG2, respectively, can be calculated and are in good agreement with those attained from the cathodic polarization curves.

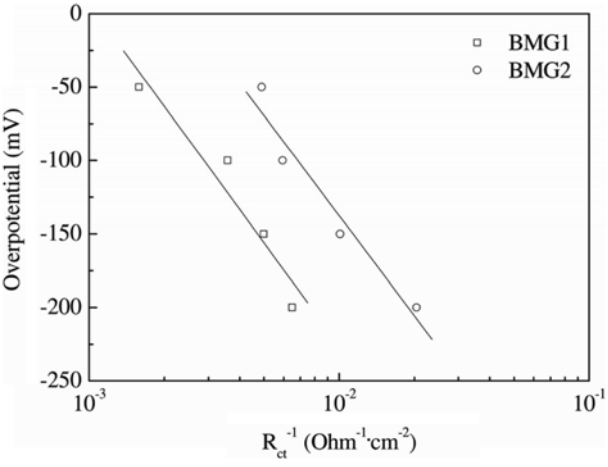

Fig. 8. The relationship of charge transfer resistance (R_{ct}^{-1}) vs. overpotential (η).

CONCLUSIONS

The new Fe-based bulk metallic glasses of BMG1 and BMG2 are fabricated using industrial raw materials and their electrochemical and electrocatalytic behaviors are characterized for hydrogen evolution in 1 M KOH solution. The results show that BMG2 exhibits high electrocatalytic activities that are further significantly improved by chemical pretreatment in 1 M HF solution, exceeding electrocatalytic activities of BMG1 and G14. With a cobalt addition, the tendency of the increase in the double layer capacitance C_{dl} and the charge transfer resistance R_{ct} for BMG1 and BMG2 is consistent with that of current density, indicating enhancement of the HER kinetics.

ACKNOWLEDGEMENTS

The work was supported by the Korean Ministry of Commerce, Industry and Energy through the project entitled as "the development of structural metallic materials and parts with super strength and high performance."

REFERENCES

1. A. Yokoyama, H. Komiyama and H. Inoue, *J. Catal.*, **68**, 355 (1981).
2. A. Baiker, R. Schlogl and E. Armbruster, *J. Catal.*, **107**, 221 (1987).
3. G. Carturan and G. Cocco, *J. Catal.*, **90**, 178 (1984).
4. G. Kisfaludi, Z. Schay and L. Guczi, *Appl. Surf. Sci.*, **29**, 367 (1987).
5. F. Albertos, B. H. Harji and C. N. Kenney, *Appl. Catal.*, **65**, 85 (1990).
6. G. Kisfaludi, K. Kazar and Z. Schay, *Appl. Surf. Sci.*, **24**, 225 (1985).
7. H. E. Alemu and K. Juttner, *Electrochim. Acta*, **33**, 1101 (1988).
8. A. Jukic, J. Piljac and M. Metikos, *J. Mol. Catal. A-Chem.*, **166**, 293 (2001).
9. K. Brunelli, M. Dabala and R. Frattini, *J. Appl. Electrochem.*, **33**, 995 (2003).
10. H. C. Brookes, C. M. Carruthers and T. B. Doyle, *J. Appl. Electrochem.*, **35**, 903 (2005).
11. P. Ekdunge, K. Juttner and G. Kreysa, *J. Electrochem. Soc.*, **138**, 2660 (1991).
12. J. Flis, H. W. Pichering and K. O. Asare, *Electrochim. Acta*, **43**, 1921 (1998).
13. C. M. Abreu, M. J. Cristobal and G. Pena, *J. Electrochem. Chem.*, **572**, 335 (2004).
14. M. A. D. Crespo, M. P. Torres and A. M. T. Huerta, *Mater. Charact.*, **56**, 138 (2006).

15. M. L. Trudeau, J. Y. Hout and R. Schulz, *Phys. Rev. B*, **45**, 4626 (1992).
16. A. Takeuchi and A. Inoue, *Mater. Trans.*, **46**, 2817 (2005).
17. M. M. Jaksic, *Int. J. Hydrog. Energy*, **26**, 559 (2001).
18. J. M. Jaksic and M. M. Jaksic, *Int. J. Hydrog. Energy*, **23**, 1121 (1998).
19. K. Asami, M. Naka and K. Hashimoto, *J. Electrochem. Soc.*, **127**, 2130 (1980).
20. M. P. M. Kaninski and V. M. Nikolic, *Int. J. Hydrog. Energy*, **34**, 703 (2009).
21. F. Rosalbino, S. Delsante and G. Borzone, *Int. J. Hydrog. Energy*, **33**, 6696 (2008).
22. M. M. Hukovic and A. Jukic, *Electrochim. Acta*, **45**, 4159 (2000).